

1 **End-to-End Flood Risk Assessment:**
2 **A Coupled Model Cascade with Uncertainty Estimation**

3 Hilary K. McMillan ^{a*} and James Brasington ^b

4 ^a National Institute of Water and Atmospheric Research Ltd, 10 Kyle St, Riccarton, Christchurch, NZ

5 ^b Centre for Catchment and Coastal Research, University of Wales, Aberystwyth, SY23 3DB, UK

6

7

8 **Abstract**

9 This paper presents the case for an ‘End-to-End’ flood inundation modelling strategy: the
10 creation of a coupled system of models to allow continuous simulation methodology to be
11 used to predict the magnitude and simulate the effects of high return period flood events.
12 The framework brings together the best in current thinking on reduced complexity
13 modelling to formulate an efficient, process-based methodology which meets the needs of
14 today’s flood mitigation strategies. The model chain is subject to stochasticity and
15 parameter uncertainty, and integral methods to allow the propagation and quantification
16 of uncertainty are essential in order to produce robust estimates of flood risk.

17 Results from an experimental application are considered in terms of their implications for
18 successful floodplain management, and compared against the deterministic methodology
19 more commonly in use for flood risk assessment applications. The provenance of
20 predictive uncertainty is also considered in order to identify those areas where future
21 effort in terms of data collection or model refinement might best be directed in order to
22 narrow prediction bounds and produce a more precise forecast.

23

25 Modern Responses to Flood Risk

26 In recent years, significant changes in scientific, public and government opinion have
27 brought about a reappraisal of flood management policy in Britain. Costly failures of
28 structural flood defence measures have highlighted the inadequacy of historical designs
29 when faced with the changing nature of river flow characteristics due to climate change,
30 urbanisation and land-use change on floodplains. This has been matched by a broadening
31 of the concept of flood risk assessment from purely economic considerations to cover
32 wider social and environmental values (DEFRA, 2002). In response to these drivers,
33 current governmental policies on flood prevention and mitigation measures increasingly
34 favour ‘soft’ solutions centring on the restoration, enhancement or creation of the natural
35 functions of the floodplain, over ‘hard’ engineering solutions.

36 The Need for an Updated Approach to Flood Risk Assessment**37 *Non-Stationarity of the Flood Generation Process***

38 Today we are in a period of what is widely considered to be enhanced flood risk caused
39 by the joint human factors of climate change and land-use change (Wheater, 2006). Non-
40 stationarity is exhibited in the recent precipitation record (Dai *et al.*, 1997; Easterling *et al.*,
41 2000; Groisman *et al.*, 2004; Huntington, 2006; Osborn and Hulme, 2002; Staeger *et al.*,
42 2003), suggesting an intensification of the hydrological cycle, and giving credence to
43 GCM model predictions of increased frequency of heavy rainfall events (Arnell *et al.*,
44 2001; Arnell and Reynard, 1996). These results may be compounded by aspects of land-
45 use change which reduce the ability of catchments to store flood water and to attenuate
46 flood peaks.

47 If non-stationarity is accepted as existing in the flood generation process, this violates a
48 critical assumption of the mathematical theory behind conventional, statistical flood risk
49 assessment. In order to derive the extreme value distribution which these methods fit to a
50 data series of recorded flood peaks, floods must be assumed to occur as independent,
51 identically distributed, random events from a single, stationary distribution. Even where
52 recurrence intervals are regularly updated with new data, the non-stationarity of the
53 process over the data collection period invalidates that assumption.

54 *Distributed Flood Risk Mapping*

55 Historically, the chief focus of flood risk assessment (FRA) has been the derivation of
56 discharge or stage for a given set of return periods, reflecting a reliance on structural
57 flood defence works whose aim was to contain flood flows within the designated channel.
58 Soft engineering solutions, floodplain restoration and homeowner responsibility demand
59 instead spatially distributed flood risk information. To cater for this demand, 1D
60 hydraulic models are typically extended to provide ‘basin-fill’ water elevation mapping
61 using either extended cross-sectional data or a network of floodplain storage cells (e.g.
62 USACE, 2006). This method typifies a more simplistic view of the floodplain as purely a
63 storage reservoir.

64 In contrast, flood defence circumvention or failure during extreme events has
65 demonstrated the connectivity of channel and floodplain as a coupled system during

66 times of flood. The hydraulic approximations made by a 1D model prevent representation
67 of lateral momentum transfer between the river and the floodplain, and cannot account
68 for the pressure gradients which force water flows at highly variable rates between the
69 two areas. The increased expectation of flood flows through complex urban areas, due to
70 changes in flood defence strategy, requires flood risk mapping based on 2D models
71 which are capable of providing a dynamic representation of water transport onto and
72 around the floodplain.

73

74

75 **Development of a Process-Based Continuous Simulation** 76 **Methodology**

77 This paper proposes a preliminary structure for a modern FRA methodology which,
78 motivated by a desire to address the deficiencies in standard FRA techniques outlined
79 above, seeks to combine the benefits of the latest modelling techniques to produce an
80 efficient, integrated approach to current FRA requirements. A central aim for the
81 structure was that it should embody a process-based approach; this greatly increases the
82 predictive power of the system in response to novel input and boundary conditions and
83 allows the structure and parameters of the system to be modified to reflect knowledge of
84 changing conditions of climate and land-use. In order to achieve this, the FRA structure is
85 underpinned by the technique of continuous simulation.

86 Continuous simulation uses the available precipitation record for the catchment as a basis
87 for creation of long synthetic rainfall series. These series are used as input to a rainfall-
88 runoff model to produce the corresponding discharge series, from which extreme event
89 frequencies may be calculated explicitly. The method provides continuous soil moisture
90 accounting which gives implicit consideration of antecedent wetness conditions in the
91 catchment. Using this flexible method, climate change might be represented via a
92 modification of the rainfall frequency distributions using estimates of the effects of
93 climate change on particular aspects of rainfall patterns. Land-use change could be
94 included via a modification of the rainfall-runoff model structure or parameters, such as
95 an increase in runoff coefficient. Although continuous simulation has previously been
96 used to forecast the discharge magnitude of extreme floods (Cameron *et al.*, 1999; Chetty
97 and Smithers, 2005; Franchini *et al.*, 2000; Hashemi *et al.*, 2000; Maskey *et al.*, 2004;
98 Onof *et al.*, 1996; Pandit and Gopalakrishnan, 1996), and in rare cases extended to
99 applications in design of structural floodplain defence measures (Hsieh *et al.*, 2006) and
100 flood mapping studies (Faulkner and Wass, 2005), it has not been considered suitable for
101 integration into the standard FRA framework due to the computational overhead required.
102 However, by using a relatively simple rainfall-runoff model, it proves to be a practical
103 and valuable tool.

104 The new structure is also defined by its integrated, 'End-to-End' approach to FRA. As
105 management plans become catchment- or basin-wide in their scope, so too should FRA
106 methods be spatially and temporally ambitious. No part of the catchment acts in isolation;
107 the process-based approach attempts to replicate the connected system through a cascade
108 of coupled models representing precipitation regime, rainfall-runoff characteristics and
109 floodplain inundation behaviour. Discharge estimates from the continuous simulation of

110 runoff are used to drive a 2D model of floodplain hydraulics which utilises new, high-
111 resolution elevation data to enable urban floodplain modelling at the smallest scales and
112 paves the way for additional modules for vulnerability and damage assessment. These
113 would be used to calculate the social and economic impacts of floods, for example using
114 information on building use or value (Apel *et al.*, 2004; Merz *et al.*, 2004), and could be
115 implemented within a risk-based sampling technique to reduce computational burden
116 (Dawson *et al.*, 2005). Finally, the coupled model structure may be run within a proven
117 uncertainty estimation framework, to allow explicit calculation of the cascading
118 uncertainties.

119 This technique has previously been tested within a reduced stochastic-rainfall-model:
120 rainfall-runoff-model system (Blazkova and Beven, 2002; 2004; Cameron *et al.*, 2000;
121 Kuchment and Gelfan, 2002; Lamb, 1999). Uncertainty estimation within a full ‘End-to-
122 End’ approach is already being successfully applied to event-based simulation (De Roo *et al.*,
123 2003; Pappenberger *et al.*, 2005; Sattler and Feddersen, 2005), although these authors
124 note the computational limitations currently placed on the method. This study places
125 particular emphasis on the need to integrate uncertainty estimates into model predictions
126 targeted for end-user communities.

127

128

Modelling and Methods

129

Overview

130 A coupled model chain is created consisting of a stochastic rainfall model, a rainfall-
131 runoff model and a floodplain inundation model. This section presents an outline of each
132 model, followed by the coupling methodology. Component models are chosen to
133 represent the latest advances in reduced-complexity methods, however flexibility is key
134 to the End-to-End FRA ethos and models could be varied according to individual case
135 attributes.

136 The model descriptions given here are necessarily brief; full detail may be found in
137 McMillan (2006) and McMillan and Brasington (2007).

138

Component Models

139

Stochastic Rainfall Model

140 All stochastic rainfall generation models rely on an initial decomposition of rainfall
141 records to identify frequency characteristics of storm data (e.g. depth, duration and
142 intensity), which are then used to parameterise a rainfall generation mechanism. A
143 profile-based method was chosen, for ease of implementation and a desire to reduce the
144 need for parameterisation by use of a ‘data-based’ method. The method splits the total
145 storm depth into time-step depths by using a profile or mass curve (e.g. Arnaud and
146 Lavabre, 1999; Beven, 1987; Blazkova and Beven, 2002; Cadavid *et al.*, 1991; Cameron
147 *et al.* 1999; 2000; Cernesson *et al.*, 1996; Diaz-Granados *et al.*, 1984; Eagleson, 1972;
148 Hebson and Wood, 1982).

149 The distributions of storm intensity, duration and inter-arrival time are collated and
150 smoothed using Gaussian kernel density estimation (Silverman, 1982; 1986; Antoniadis,

151 1995), with modifications made for skewed or discontinuous distributions as appropriate.
 152 In order to create the stochastic storm sequence, random samples were drawn from these
 153 distributions, and a storm created using a profile drawn randomly from the storm record.
 154 Two modifications were made to this basic model structure to improve model
 155 performance, as follows.

156 Firstly, storms may be segregated by season if characteristic differences exist (e.g.
 157 Blazkova and Beven, 2000; Walshaw, 1994). Here a split into two seasons was made
 158 (Feb-Aug, Sep-Jan) to reflect seasonality in rainfall totals. Secondly, the storm
 159 characteristics showed a negative correlation between intensity and duration, which
 160 should be recognised within the model structure to optimise performance (Cameron *et al.*,
 161 1999; 2000; Goel *et al.*, 2000; Kurothe *et al.*, 1997). The empirical intensity distributions
 162 were therefore split by duration into 5 classes before sampling, this method being chosen
 163 in preference to the use of a bivariate intensity-duration sampling distribution to avoid
 164 limitation of model stochasticity. An additional modification to extend the tail of the
 165 intensity distributions using a fitted extreme value distribution, in order to accommodate
 166 the possibility of more intense events than those in the recorded sequence, was rejected
 167 after trials showed that it caused overestimation of observed maximum rainfalls.

168 **Rainfall-Runoff Model**

169 A transfer function methodology was chosen to provide the rainfall-runoff component of
 170 the model chain. This popular class of models originates from unit hydrograph theory and
 171 the Nash Cascade (Nash, 1959), and represents the catchment as a linear system of
 172 interconnected flow pathways, modified by a nonlinear transform to represent runoff
 173 generation. This model type combines the benefits and well-conditioned nature of a
 174 lumped model while allowing knowledge of catchment structure to be incorporated into
 175 model definition. Various versions of this model have been implemented (e.g. Jakeman *et al.*,
 176 1990; Young and Beven, 1991; 1994 and a comprehensive review by Young, 2003);
 177 the version described by Sefton and Howarth (1998) was used here.

178 The equations governing the non-linear rainfall transform are as follows:

$$179 \quad u_t = R_t(S_t + S_{t-1})/2 \quad (1)$$

$$180 \quad S_t = cR_t + \left[1 - \frac{1}{\tau(T_t)}\right]S_{t-1} \quad (2)$$

$$181 \quad \tau(T_t) = \tau_w \cdot \exp(20f - T_t f) \quad (3)$$

182 Where u_t is the volume of effective rainfall at time t resulting from input rainfall R_t . S_t
 183 represents the catchment storage index at time t , $\tau(T_t)$ is the recession rate of S_t at
 184 temperature T_t which depends on the recession rate at 20°C, τ_w . The parameter c ensures
 185 equality of effective rainfall and runoff volumes. Parameter f modulates
 186 evapotranspiration with temperature, requiring an input temperature series.

187 The linear routing module of the rainfall-runoff model uses a transfer function to convert
 188 effective rainfall u_t into flow Q_t . The most usual form of transfer function to be specified
 189 for small catchments consists of two parallel pathways representing quickflow and
 190 slowflow. This choice of model structure was accepted for the study catchment, after

191 consideration of physical catchment characteristics and gauging carried out in the field,
 192 together with model trials. The model structure is shown in Equation 4.

$$193 \quad Q_t = \frac{b_0 + b_1 \cdot z^{-1}}{1 - a_1 \cdot z^{-1} - a_2 \cdot z^{-2}} \cdot u_{t-\delta} = \left[\frac{\beta_q}{1 - \alpha_q \cdot z^{-1}} + \frac{\beta_s}{1 - \alpha_s \cdot z^{-1}} \right] \cdot u_{t-\delta}$$

194 *Equation 4: Two-component transfer function structure*

195 Where z^{-1} is the backward shift operator, i.e. $z^{-1}Q_t = Q_{t-1}$. The parameters that must be
 196 estimated are β_q , β_s , α_q , α_s , δ (where suffix q represents quickflow parameters, s
 197 represents slowflow parameters), given calibration data consisting of effective rainfalls
 198 $\{u_t\}$ and flows $\{Q_t\}$. The parameters for both non-linear and linear model parts are
 199 estimated using the GLUE procedure (Beven and Binley, 1992) outlined below.

200 **Floodplain Inundation Model**

201 The floodplain inundation model chosen for this application takes advantage of
 202 significant recent progress in reduced complexity modelling, achieved by directly
 203 coupling 1d channel hydraulic models with 2d raster storage cell approximation for
 204 floodplain flows (e.g., Bates and De Roo, 2000). This approach offers order of magnitude
 205 gains in computational efficiency over more complex finite element and volume codes
 206 (Aronica, *et al.*, 2002; Horritt and Bates, 2001b).

207 The channel model uses the kinematic approximation to the Saint-Venant equations,
 208 which describe one-dimensional unsteady open channel flow. They consist of a
 209 continuity equation and a momentum equation (Equations 5 and 6). Variables used are:
 210 Q , flow; A , cross-sectional area; t , time; x , horizontal position; y , vertical position; g ,
 211 gravity; S_0 , bed slope; S_f , friction slope.

212

$$\text{Continuity Equation: } \frac{\partial Q}{\partial x} + \frac{\partial A}{\partial t} = 0 \quad (5)$$

$$\text{Momentum Equation: } \underbrace{\frac{1}{A} \cdot \frac{\partial Q}{\partial t}}_{\text{Local Acceleration Term}} + \underbrace{\frac{1}{A} \cdot \frac{\partial}{\partial x} \left(\frac{Q^2}{A} \right)}_{\text{Convective Acceleration Term}} + \underbrace{g \frac{\partial y}{\partial x}}_{\text{Pressure Force Term}} - \underbrace{g(S_0)}_{\text{Gravity Force Term}} - \underbrace{S_f}_{\text{Friction Force Term}} = 0 \quad (6)$$

213 The kinematic approximation uses the full continuity equation, but only the gravity and
 214 friction force terms in the momentum equation, neglecting pressure and acceleration
 215 terms.

216 The floodplain model uses a raster cell approach that has been popularised by Bates and
 217 De Roo (2000) and De Roo *et al.* (2000) with their model LISFLOOD-FP; similar ideas
 218 have also been used by Estrela and Quintas (1994) and Romanowicz *et al.* (1996), all
 219 building on methods suggested by Cunge *et al.* (1976). The model uses numerical
 220 discretisation in space and time, as with the channel model. The floodplain is treated as a
 221 grid of square cells, with flow allowed between 4-connected cells. As in the channel

222 model, continuity and momentum equations are solved to calculate flow rates. The
 223 continuity equation relates flow across cell boundaries to the volume stored in the cell
 224 (Equation 7); the momentum equation uses Manning's Law to relate flux to surface slope
 225 and hydraulic radius (Equation 8).

226

$$\text{Continuity Equation: } \frac{\partial h^{i,j}}{\partial t} = \frac{Q_x^{i-1,j} - Q_x^{i,j} + Q_y^{i,j-1} - Q_y^{i,j}}{\Delta x \Delta y} \quad (7)$$

$$\text{Momentum Equation: } Q_x^{i,j} = \frac{h_{flow}^{5/3}}{n} \left(\frac{h^{i-1,j} - h^{i,j}}{\Delta x} \right) \Delta y \quad (8)$$

227 Where $h^{i,j}$ is water depth at cell (i,j), h_{flow} is free water depth between two cells, Δx and Δy
 228 are the cell dimensions, n is Manning's friction coefficient, and Q_x and Q_y are the flow
 229 rates in two directions between cells.

230 Two major modifications are made to this basic model structure; both are described more
 231 fully in McMillan and Brasington (2007). Firstly, the numerical stability of the model is
 232 improved using a redesigned function to limit excessive flows between cells, which occur
 233 particularly in areas of deep, ponded water due to the use of numerical approximations to
 234 the governing differential equations. This limiter aimed to improve on that designed by
 235 Hunter *et al.* (2004), by recognising the interaction of multi-directional flow paths and
 236 hence retaining information on preferential flow pathways within the floodplain. This
 237 was achieved by imposing a total outflow limit on each cell to be split proportionally
 238 between the multiple outflows; implicitly considering these flows as dependant processes.
 239 The limiter form is shown in Equation 9. The use of a limiter removes model sensitivity
 240 to floodplain friction, a pattern previously noted in storage cells models, and arises
 241 because the form of the flow limiter becomes the dominant control on floodplain flows
 242 (Romanowicz and Beven, 2003; Hunter *et al.*, 2004; Hall *et al.*, 2005).

$$243 \quad Q_x^{i,j} = \min \left\{ Q_x^{i,j}, \underbrace{\left(\frac{Q_x^{i,j}}{Q_x^{i,j} + Q_x^{i-1,j} + Q_y^{i,j} + Q_y^{1,j-1}} \right)}_{\text{Proportion-of-flow}}, \underbrace{\left(\frac{\min \{H_x^{i,j}, H_x^{i-1,j}, H_y^{i,j}, H_y^{i-1,j}\} \Delta x \Delta y}{1 + 1 / (\text{Number-of-Outflows})} \right)}_{\text{Max-total-outflow-before-surface-gradient-is-reversed}}, \underbrace{\left(\frac{Q_x^{i,j} \cdot h^{i,j} \cdot \Delta x \Delta y}{(Q_x^{i,j} + Q_x^{i-1,j} + Q_y^{i,j} + Q_y^{1,j-1}) \cdot \delta x} \right)}_{\text{Outflow-required-to-empty-cell}} \right\} \quad (9)$$

244 Secondly, the model is upgraded to allow sub-grid model parameterisation, in an attempt
 245 to harness the wealth of terrain information contained within a LIDAR scan of a river
 246 reach within an efficient model structure. This is achieved by using the concept of 'cell
 247 porosity' to allow the use of sub-grid topographic information within a coarse resolution
 248 model. The porosity function quantifies the percentage of the assumed cell volume that is
 249 available for water storage after accounting for sub-grid features; similarly modified
 250 values of cell boundary cross-section area and wetted perimeter are also defined. By
 251 using this information to adjust the continuity and momentum equations, model
 252 behaviour may react to preferential flow directions and flow volumes in a way that is not
 253 possible using a simple roughness coefficient. The method is designed to reflect the first
 254 order controls on flow conveyance while enabling simulations to be carried out at a

255 computationally efficient resolution; Yu and Lane (2006) demonstrate the potential of the
256 concept by using sub-grid scale information at a resolution half that of the model.

257 **Model Coupling**

258 ***Using GLUE in End-to-End Hydrological Modelling***

259 The GLUE technique (Beven and Binley, 1992) is a tool for investigation of model
260 response and associated uncertainty, under equifinality of model structure or
261 parameterisation. Based on principles from Bayesian statistics, the technique relies on the
262 computation of a 'likelihood' measure, an estimate of how likely the model is to produce
263 acceptable simulations based on its performance tested against some observed data. The
264 model is run many times using many different parameter sets (often chosen using Monte
265 Carlo analysis), and the predictions of each behavioural model are weighted using a
266 normalised likelihood value. A cumulative distribution can then be calculated for each
267 prediction variable at each timestep, and hence quantiles as required (Equation 10).

$$268 \quad P(Q_t < q) = \sum_{i \in X} L(\Theta_i) \text{ where } X = \{i \mid Q_t^i < q\} \quad (10)$$

269 Where Q_t is the predicted flow (or other variable) at time t , q is the observed flow, Θ_i is
270 the i^{th} set of parameters for the model, $L(\Theta_i)$ is the likelihood value obtained when the
271 model is run using these parameters, and Q_t^i is the predicted flow at time t using these
272 parameters. The advantages of the technique lie in the ability to make predictions of
273 uncertainties in highly non-linear systems where the assumptions of traditional statistical
274 techniques prove too restrictive.

275 It is important to note that when estimating confidence limits using GLUE, the discharge
276 predictions at each timestep do not relate to a single set of parameter values and hence a
277 single model realisation. Thus when applying GLUE to coupled models, uncertainty
278 bounds cannot be cascaded through the model series by treating the bounds for output
279 timeseries as a prediction relating to a single parameter set that may be input into the
280 following model. Instead, results relating to each parameter set must be propagated
281 through the model chain individually, the resulting computational demands presenting
282 serious constraints on the number of dimensions over which uncertainty can be
283 considered. Decisions therefore had to be made in order to restrict the scope of the
284 analysis, balancing the efficiency of the system against the extent and accuracy of the
285 results.

286 ***Coupling of Rainfall and Rainfall-Runoff Models***

287 The rainfall simulation model was derived using empirical data rather than fitted
288 parameters, and therefore there is no explicit parameter uncertainty. Instead, the
289 perceived uncertainty in a rainfall simulation relates to the choice of model type and the
290 inherent stochasticity of the model; one realisation of a rainfall series represents only a
291 single possible outcome. We therefore consider the uncertainty in realisation of rainfall
292 series, together with the uncertainty of choice of rainfall-runoff model parameters. Model
293 structural uncertainty is not considered here, although it is inherent in the choice of each
294 component model.

295 Although the most comprehensive approach to uncertainty estimation would be to search
296 these two sources of uncertainty as a 2D parameter space (i.e. every rainfall realisation
297 coupled with every parameter set), this strategy would be extremely costly in
298 computational terms. Instead, following Cameron et al. (1999), independent random
299 selections are made from the two sets, and this joint Monte Carlo sample assigned a
300 performance weighting from the rainfall-runoff model parameter set since the weightings
301 of the rainfall simulations are deemed equal.

302 ***Coupling of Rainfall-Runoff and Floodplain Hydraulic Models***

303 The rainfall-runoff model is used to process each series of simulated rainfall to yield an
304 estimate of channel discharge at the upstream boundary of the inundation model. The
305 models must be coupled in such a way as to allow the uncertainty in discharge series to
306 be represented in the input to the floodplain hydraulic model; the aim being to achieve
307 inundation extent estimation at various return periods, while specifying the uncertainty
308 associated with the predictions. The most complete technique for estimating this
309 uncertainty would be to route the discharge predicted by each rainfall simulation /
310 rainfall-runoff model combination through the floodplain hydraulic model. Unfortunately
311 this is clearly not a practical proposition due to computation restrictions.

312 However, by careful choice of assumptions with regard to the flow behaviour at the site,
313 efficient methods for estimation of inundation frequency are possible. Here, an approach
314 based on three key assumptions is proposed.

315 • First, it is assumed that the inundation extent related to a particular flow event is
316 independent of flow conditions prior to the time at which out-of-bank flow began. This is
317 justified due to the rarity of closely spaced flood events, and allows modelling of
318 individual events to replace the need for continuous simulation.

319 • Secondly, it is assumed that the frequency distribution of inundation extent may be
320 characterised using an annual maximum series for flow events, rather than requiring a
321 peaks-over-threshold (POT) analysis. This is a reasonable assumption given a long
322 simulated data series: Robson and Reed (1999) show that the advantage gained by using
323 POT data can typically be acquired using one additional year of annual maximum data.

324 • A third assumption is made that the event in each year which causes the greatest
325 inundation is that which has the greatest instantaneous peak discharge. This is based on
326 the premise that the magnitude of an event is a good indication of other damaging
327 attributes of a flood such as over-bank volume or duration (the strong peak flow : volume
328 relationship found in the test catchment is described in the results section). This
329 assumption is key to reducing processing time as the storm with maximum discharge in
330 each hydrological year can be easily identified. In contrast, identifying the storm causing
331 most inundation from a flow series would be a challenging and time-consuming task, and
332 might not be possible without carrying out the inundation simulation in full.

333 A final decision was taken that uncertainty in calibration of the floodplain model, i.e.
334 value of Manning's n for channel friction, would not be part of the coupled uncertainty
335 analysis. If this were to be undertaken, then for each return period of interest, the design
336 event corresponding to each discharge series realisation would have to be propagated
337 through the inundation model with each possible value of channel friction, giving rise to

338 tens of thousands of simulations. This is not computationally feasible given that each
339 inundation simulation takes several hours to perform (235 minutes benchmarked on a
340 Pentium 4, 3.2 MHz PC with 1.5GB RAM, based on simulations with the optimal
341 channel friction coefficient, $n = 0.05 \text{ m}^{-1/3}\text{s}$). Instead, by considering only the
342 uncertainty from the rainfall and rainfall-runoff models, the confidence bounds on the
343 design event magnitude may be translated directly into confidence bounds on inundation
344 extent. A limited sensitivity analysis of the model response to uncertainty in channel
345 friction is, however, undertaken to provide a gauge of its relative effects on the
346 inundation predictions. There is clear scope for this additional uncertainty source to be
347 more fully considered; however at present this simplified analysis is thought reasonable
348 as unlike the strongly equifinal behaviour of the rainfall-runoff model, the hydraulic
349 model calibration showed a unimodal performance distribution with a single optimal
350 value when validated against combined inundation and hydrograph data.

351 ***Process Methodology***

352 Drawing on the assumptions outlined above, the process methodology may thus be
353 described. Simulated rainfall series, of a length appropriate to the design event to be
354 estimated, are produced using the stochastic rainfall model. One series is generated to
355 correspond to each rainfall-runoff model parameter set, the number of which must be
356 chosen by the investigator. These sets are randomly created by sampling from the feasible
357 parameter ranges. Each set is assigned a performance ('likelihood') value corresponding
358 to its ability to correctly reproduce a flow record. In the test application described below,
359 the parameter sets are validated using an 11-year rainfall-flow record. The fit between
360 observed and predicted flow is tested using the R^2 criterion (Nash and Sutcliffe, 1970),
361 and the parameter set is rejected for values < 0.6 .

362 Each rainfall series is routed through the rainfall-runoff model run with the corresponding
363 parameter set. On completion of this step, a set of T-year discharge estimates is therefore
364 available by reading directly from a listing of the maximum flow in each simulated year.
365 For each rank position in the series, the set of possible realisations of discharge value is
366 ordered and associated with the parameter set performance value. A weighted cumulative
367 distribution of discharge for each of these return periods can therefore be created, and
368 upper and lower limits at the required confidence level together with any other quantiles
369 produced by interpolation.

370 The discharge alone is insufficient to create the flow hydrograph required for input into
371 the floodplain inundation model. The hydrograph is therefore produced using a triangular
372 approximation, based on an empirical flow-volume relationship derived for the
373 catchment, together with standard percentages of flow volume before and after the peak
374 Trials showed that this method was effective in providing accurate estimation of flood
375 volumes.

376

377

Test Application

378 ***Upper Granta Catchment***

379 This section sets out a trial application of the end-to-end forecasting methodology, based
380 on a 2 km reach of the River Granta in Cambridgeshire, UK, which has a long history of

381 flooding. Full details of the reach and catchment hydrology are presented in McMillan
382 (2006). The catchment is characterized by agricultural land with gentle gradients and lies
383 on a chalk aquifer overlain by Boulder Clay. Channel widths through the study reach are
384 typically 5-10 m with slopes in the order of 0.5% and thus within the appropriate limits
385 for a kinematic approximation of channel hydraulics (Woolhiser and Liggett, 1967). The
386 study reach straddles the town of Linton which has been frequently affected by severe
387 flooding, most recently during October 2001. In this event, flooding occurred when 90
388 mm of rain fell in 17 hours onto an already raised water table and caused extensive
389 damage to 72 properties, including key historic buildings in the town centre. Estimates of
390 the return period for this event range from 100 – 400 years (Halcrow, 2005; McMillan,
391 2006). Records from this event were used to parameterise the floodplain inundation
392 model; 15-year rainfall and discharge records from the catchment were used to create the
393 stochastic rainfall model and to assign performance values for each rainfall-runoff model
394 parameter set. The aim of the trial was to allow inundation hazard mapping for long
395 return-period events, and therefore rainfall series of 1000 years were used. These were
396 then processed to obtain predictions of discharge at yearly return periods up to 1000
397 years, and inundation extent at a range of return periods: 10, 50, 100, 500 and 1000 years.

398

399

Results

400 Discharge Prediction

401 The discharge series produced from the coupled stochastic rainfall and rainfall-runoff
402 models were used to produce cumulative distributions of discharge, plotted in Figure 1A,
403 and shown in detail in Figure 1B for comparison with the 2001 flood.

404

405

406

407

408

409

410

Figure 1: Modelled Discharge: Return Period Relation. A. Full Range. B. Detail. Dashed Lines show (a) Discharge associated with 2001 flood, with return period estimated from median and quartiles and (b) Discharge associated with 100-year flood.

411 The results demonstrate the high level of uncertainty associated with predictions made
412 using the simulated rainfall series and rainfall-runoff model. For example, the 90%
413 confidence interval for the 100-year flood discharge is $14.8 - 48.0 \text{ m}^3\text{s}^{-1}$ (Figure 1B), a
414 large uncertainty in terms of flood hazard or in the cost-benefit ratio of any flood
415 protection works. Similarly, estimates the return period of the October 2001 flood (20.5
416 m^3s^{-1}) range from 7 to 146 years between the 5% and 75% quartiles (the return period
417 estimated from the upper 90% bound was not captured).

418

419 Hydrograph Formation

420 The hydrograph for each return period (10, 50, 100, 500 and 1000 years) at the 5%, 50%
421 (median) and 95% percentiles was formed according to the empirical flow-volume
422 relationship found (Equation 11).

423

$$\text{Volume} = 36720 * \text{Flow}^{1.35}$$

424

Equation 11: Regression Relationship between Peak Flow (m^3s^{-1}) and Volume (m^3)

425

The strong correlation found between flow and volume (correlation coefficient 0.90) justifies the use of a standardised hydrograph based on peak value. As an example, the hydrographs for the 1000-year flood are shown in Figure 2.

426

427

428

429

430

Figure 2: Design Hydrographs for the 1000-year return period, at the 5%, 50% and 95% points of the cumulative distribution

431

432

433

434

435

Inundation Extent

436

The design hydrographs give discharge series for the gauging station at Linton, upstream of the town centre, forming the upstream boundary condition for the hydraulic model. Following model evaluation, the floodplain code was implemented at 10 m resolution using the sub-grid porosity treatment for maximum computational efficiency. The channel friction coefficient (Manning's n) was set at $0.05 m^{-1/3}s$, which gave optimal performance judged using a multi-criteria validation for the 2001 flood event. This validation was based on a weighted combination of performance measures in hydrograph simulation and inundation behaviour. Downstream hydrographs were judged according to accuracy of peak discharge magnitude and timing; inundation simulations were validated using a fuzzy performance measure which tested flood depth prediction for each inundation property, while allowing a margin of error for perceived reporting inaccuracies. For each return period, the hydraulic model was used to produce an inundation simulation relating to the design hydrographs for the 5%, 50% and 95% points of the distribution of peak discharge magnitudes. The results are shown in Figure 3.

437

438

439

440

441

442

443

444

445

446

447

448

449

450

451

452

Figure 3: Areas of Predicted Inundation at the 5%, 50% and 95% points of the cumulative distribution of peak discharge magnitudes

453

454

455

456

457

Communication of Results

458

The spatial pattern of inundation extent evident in Figure 3 is ultimately constrained by the valley morphology, so that despite large differences in the peak discharges of the extreme return periods, the maximal inundation envelope remains comparatively consistent. This is due to relatively steep topography at the natural boundaries of the floodplain which serves to constrain flood waters. However, it is also at this boundary that accuracy in prediction becomes more critical, as beyond the edge of the floodplain, density of housing increases dramatically. On the floodplain itself, there are few buildings, as waterlogged land and frequent flooding have constrained construction.

459

460

461

462

463

464

465

466 This illustrates the importance of presenting results in a method sensitive to the intended
467 use. Mapped inundation extents (Figure 3) would be useful for strategic and emergency
468 planning at the local scale, e.g. preparation of emergency evacuation and traffic routing
469 plans. However, for applications such as a benefit-cost analysis for a structural flood
470 defence scheme, derived statistics such as number of houses flooded may present the
471 trends more clearly (Figure 4). Further analysis could count only houses flooded beyond
472 the protection limits of sandbags or removable floodgates.

473

474

475

476

477

478

Figure 4: Number of houses flooded (to any depth) as a function of return period and percentage point of peak discharge distribution

479

480 Figure 4 demonstrates a sharp rise in the number of properties flooded between the 10-
481 100 year events; then a smaller increase up to the 1000-year event. This might suggest a
482 threshold return period beyond which the expenditure involved in containing the Granta
483 would not be realised in terms of damage saving. A worthwhile extension of the current
484 work would be to link the properties in the area to a valuation, perhaps through zoning by
485 postcode, in order to estimate the financial cost of each flood event. This could be
486 achieved using depth-damage curves tailored to building type. Depth mapping would also
487 be useful to aid identification of areas of high risk to life and greater damage to property.
488 Calculated variables such as area and number of houses inundated could be used directly
489 within the UK government system for assessment of future flood defence engineering
490 works (DEFRA, 2002).

491

492

493

Constraining Uncertainty in End-to-End Modelling

494

Constraining Uncertainty in Discharge

495

496

497

498

Quantifying the uncertainty in discharge prediction and analysing its provenance offers the scope to determine the main sources of uncertainty, and identify means of uncertainty reduction through refinement of model structure, parameterisation or boundary condition specification. Two example uncertainty sources are considered here.

499

Effects of Uncertainty in Rainfall Series

500

501

502

503

504

505

506

Part of the uncertainty in discharge is due to the stochasticity of precipitation patterns that force the model chain, simulated here via the ensemble of 1000 climate scenarios. To consider the reduction in uncertainty if improved knowledge of future rainfall behaviour was available, we simulate the extreme case where the full 1000-year rainfall series is known exactly. The Monte Carlo simulations are re-run using a single random ‘correct’ series, with each rainfall-runoff model parameter set as before (Figure 5).

507
508
509
510
511
512

Figure 5: Modelled Discharge: Return Period Relation, using single rainfall series. (a) Full Range. (b) Detail. Dashed Line shows discharge associated with 2001 flood, with return period estimated from median and quartiles.

513

514 The return period-flow curves are less smooth than previous results, representing the
515 increased dependence on model response to particular rainfall events. The 90%
516 confidence bounds for the 100-year discharge are only slightly reduced, from [14.8, 48.0]
517 to [14.8, 42.4] m^3s^{-1} (Figure 5B), indicating that rainfall uncertainty has only a small
518 impact on long term discharge prediction. However, the estimate of a particular quantity
519 may be altered by a significant margin, e.g. the 2001 flood is estimated as having a return
520 period of 47.4 years instead of 33.7. The limited effect of uncertainty in precipitation
521 patterns however ultimately reflects the derivation of the rainfall model from a single 15-
522 year gauged record. A longer rainfall series might contain implicit non-stationarity that
523 exerts a significant control on discharge response.

524 ***Effects of Uncertainty in Rainfall-Runoff Model***

525 To test the effect of uncertainty in rainfall-runoff model parameterisation, the suite of
526 model simulations were rerun, using the original set of rainfall series, but the single
527 rainfall-runoff parameter set with the optimal value of the performance measure (Figure
528 6). This mimics the situation where there is no uncertainty in the rainfall-runoff model
529 parameterisation.

530
531
532
533
534
535
536

Figure 6: Modelled Discharge: Return Period Relation, using optimised rainfall-runoff model parameters. (a) Full Range. (b) Detail. Dashed Line shows discharge associated with 2001 flood, with return period estimated from median and quartiles.

537

538 In this situation, discharge estimate uncertainty is greatly reduced, e.g. the 90%
539 confidence interval for the 100-year flood discharge is constrained from [14.8, 48.0] to
540 [17.5, 20.8] m^3s^{-1} , a significant advantage for any planning of flood defence works.
541 However, this analysis must not be confused with the results of using a single set of
542 parameters without justification. Many of the alternative parameter sets had a
543 performance value very close to the optimum, giving little reason to suppose that one set
544 should be accepted against the rejection of all others. Discounting these other possible
545 flow values may have particularly damaging consequences as the confidence limits fall at
546 the lower end of the range of the wider bounds; the optimum set does not necessarily give
547 values bracketing the median of the complete uncertainty analysis.

548 **Propagating Uncertainty through Inundation Simulations**

549 The preceding section analysed the relative effects of uncertainty in the rainfall input and
550 rainfall-runoff model parameters. To understand how such changes in discharge

551 prediction distributions would affect inundation predictions in the coupled model
552 structure, the uncertainty was propagated through the hydraulic model, as before (Figure
553 7). The 100-year event only was considered, as a standard for comparison.

554 • Plot (a) shows the original analysis of the 100-year flood, repeated for comparison.

555 • Plot (b) shows the significant reduction in uncertainty of flood boundary position
556 possible if the rainfall-runoff model parameters could be defined exactly. Although this is
557 unlikely due to equifinality in parameter sets, caused by model structural deficiencies and
558 limited calibration data, it demonstrates that significant benefits could be achieved by
559 further work to reduce the number of models considered behavioural.

560 • Plot (c) shows the small reduction in uncertainty achievable if the future rainfall
561 patterns were known exactly, however the relatively minor impact compared with that of
562 Plot (b) suggests that improvements in rainfall-runoff modelling should take precedence
563 over improvements in rainfall characterisation.

~~564~~

566

567 **Figure 7:** Areas of Predicted Inundation at the 5%, 50% and 95% points of the cumulative
568 distribution of peak discharge magnitudes for the 100-year flood, using three
569 alternative methods to calculate uncertainty bounds.
570

571

572 ***Sensitivity to Inundation Model Parameterisation***

573 As discussed, uncertainty in the channel friction parameter used to calibrate the
574 floodplain inundation model was not considered due to computational constraints.
575 However, a decoupled ‘sensitivity analysis’ was undertaken to assess the relative scale of
576 this uncertainty.

577 For each return period, the 50% (median) hydrograph was routed through the floodplain
578 using channel friction coefficients of 0.04 and 0.06 m^{-1/3}s, chosen to surround the
579 previously selected optimum of 0.05 m^{-1/3}s which represented a single, global maximum
580 in the validation statistic response space. More extreme values were found to depress
581 validation scores. Inundation envelopes from the 100-year flood (Figure 8) show that
582 varying the friction parameter value within the specified range has a relatively small
583 effect relative to the uncertainty sources previously considered. It should however be
584 understood that a simplistic analysis of this kind cannot represent the nonlinear effects of
585 uncertainty propagation through the model chain, and hence provides only a guide as to
586 the likely effect of uncertainty on model results in a full application of the GLUE
587 procedure to the coupled model system.

588

589

~~590~~

592

593 **Figure 8:** Variation in inundation envelope: Comparison of (a) Uncertainty in rainfall and rainfall-
594 runoff model parameters and (b) Uncertainty associated with floodplain model channel
595 friction parameter
596

597
598

599
600

Comparison with Standard Analysis

601 To illustrate the characteristic differences of the End-to-End FRA framework from
602 conventional methodologies, the inundation predictions made using the new method are
603 compared with those of a standard FRA, carried out by the UK Environment Agency
604 which is responsible for flood management at the trial site (Bullen Consultants, 2002;
605 Halcrow 2003; 2004). The methods used are those currently recommended in the Flood
606 Estimation Handbook (Robson and Reed, 1999): a standard text which provides guidance
607 widely used in planning scenarios and engineering applications. In brief, hydrographs are
608 produced using a dual method. Firstly, hydrograph shape is produced by routing a design
609 rainfall event through a rainfall-runoff model. Five flood events during the period 2000-
610 2001 are used to estimate the parameters of this model. Secondly, discharge magnitude is
611 calculated using statistical methods. The discharge record is augmented using a 'pooling
612 group analysis' which identifies hydrologically similar catchments based on catchment
613 area, average annual rainfall and baseflow regime; priority is given to catchments close to
614 the study site. In the case of Linton, 17 other sites are used, giving a combined total of
615 486 years of record. Using this extended data set, the flood frequency curve is
616 constructed by fitting a 3-parameter Generalised Logistic Distribution to the data, with
617 cumulative distribution function as follows:

618
$$F(Q; k, \alpha, \xi) = \left[1 + \left(1 - \frac{k}{\alpha} (Q - \xi)^{1/k} \right) \right]^{-1} \quad (k \neq 0) \quad (\text{Equation 12})$$

619 The resulting discharge estimate is used to scale the hydrograph from the rainfall-runoff
620 model. This provides an upstream boundary condition for a 1D hydraulic inundation
621 model, based on cross-sectional data and created using ISIS modelling software
622 (Wallingford Software Ltd, 2006), to route flow along the channel and overbank.

623 The contrasting nature of the techniques is reflected in the predictions of the 100-year
624 discharge: $10.2 \text{ m}^3\text{s}^{-1}$ in the standard model versus $25.1 \text{ m}^3\text{s}^{-1}$ median prediction in the
625 end-to-end model, which manifest themselves in the inundation envelope forecasts
626 (Figure 9). The difference stems from the constrained design event methodology of the
627 standard analysis, such as an inability to include information on antecedent wetness
628 conditions. However most notable is an over-reliance on the gauged floodplain record in
629 the statistical flood frequency analysis, which does not allow for measurement errors such
630 as drowning of flow gauges during flood, as is known to happen at the trial site. In
631 contrast, the end-to-end technique is able to compensate for such malfunctions using the
632 correctly recorded rainfall data together with the calibrated rainfall-runoff model. This
633 situation demonstrates the valuable way in which an integrated, end-to-end methodology
634 can add value to short or censored methods by using models to capture information on

635 physical catchment processes. In addition, a more complex pattern of inundation is
636 predicted when using the new method with a 2D model, showing flow paths within the
637 floodplain and high resolution definition of the flood boundary.

638 The large difference in predictions of flood envelope has the potential to lead to very
639 different approaches to flood risk mitigation. The representation of uncertainty within the
640 end-to-end forecast also enables a more comprehensive consideration of possible flood
641 scenarios which is not possible using the results of the standard analysis technique.

642

644

645 **Figure 9:** Comparison in 100-year flood envelopes predicted using the proposed End-to-End
646 method versus a standard statistical method using the 1D ISIS flood model

647

648

649

Discussion

650 This paper set out to design a novel, flexible, process-based FRA methodology, relying
651 on a chain of coupled models running within a proven uncertainty-estimation structure. A
652 number of key findings are made. First, the benefits of extending the flood frequency
653 analysis beyond discharge magnitude estimates to include inundation simulations were
654 demonstrated. By integrating a hydraulic model into the coupled model cascade,
655 hydrologists gain the opportunity to explore the relationships between discharge,
656 inundation extent, flow paths, and likely damage to infrastructure and buildings. This is
657 especially relevant in the light of recent trends away from structural flood defences and
658 towards a greater reliance on integrated catchment management approaches which aim to
659 manage a 'functional floodplain'.

660 An important aspect of the modelling procedure is the rejection of the principle of using
661 deterministic forecasts. These are replaced by results in the form of distribution quantiles,
662 which are presented as hazard maps to allow an intuitive interpretation of the effects of
663 uncertainty on flood forecasts. Maps showing the confidence intervals allow an
664 assessment of which areas of the floodplain are most sensitive to uncertainty in discharge
665 predictions due to channel shape and local topography. Although the inclusion of
666 uncertainty estimates in a flood frequency analysis is still a relatively rare occurrence
667 outside academic research, its importance was demonstrated here: a deterministic model
668 using a single set of rainfall-runoff model parameters was shown to give biased and
669 under-predicted estimates of flood hazard. In this study, computational restraints forced a
670 reduced set of hydraulic model simulations, however it is hoped that in the future the
671 methodology could be extended to include uncertainty in hydraulic model
672 parameterisation as part of the full GLUE application. While it would not be practical to
673 propagate predictions from each discharge series through the hydraulic model, a concept
674 such as that of functional similarity (Pappenberger et al., 2005) might be used to reduce
675 computational effort. This complementary approach makes alternative choices to the
676 method outlined here: rather than simplifying the coupling procedure between
677 consecutive models, instead the number of rainfall-runoff model parameter sets is
678 severely restricted, by classification according to the type of hydrograph forms produced.

679 A wider reporting of the effects of uncertainty on model predictions may also provide an
680 impetus for further data collection in order to constrain uncertainty. By emphasising that
681 observed floods may fall within wide prediction bounds rather than the more simplistic
682 interpretation that the deterministic model is 'wrong', it becomes more obvious how
683 additional data could aid future predictions. In this study, results showed that the major
684 cause of uncertainty was equifinality in rainfall-runoff model parameterisation, and
685 therefore suggests that future effort might best be directed at reducing the range of
686 behaviour associated with the set of behavioural rainfall-runoff models. These more
687 detailed conclusions are, however, dependant on the models and coupling methods
688 chosen for the trial study, also the range of parameters and uncertainty sources that were
689 analysed.

Conclusion

690

691 This paper presents the argument for process-based FRA methodology based on
692 continuous simulation within the context of a chain of coupled models. Taking advantage
693 of advances in data provision, and reduced complexity modelling techniques, high-
694 resolution flood inundation simulation is included as part of the model chain. Such a
695 strategy is highly desirable in an age where non-stationarity of the flood generation
696 process, together with changing approaches to flood mitigation, have rendered traditional
697 statistical FRA techniques increasingly obsolete.

698 Uncertainty estimation was included as an integral part of the procedure, to assess
699 stochasticity and parameter uncertainty within the model chain. Results from a trial flood
700 frequency analysis showed that significant uncertainty was present in estimates of flood
701 extent, and indicated where future work might reduce this most effectively. The current
702 use of deterministic flood risk analyses was found to be unduly restrictive and likely to
703 give biased estimates of flood risk.

704

705

706

References

- 707 Antoniadis, A., 1995. Matlab Smoothing Toolbox. <http://www.unizh.ch/biostat/Software/>, Zurich.
- 708 Apel, H., Thielen, A.H., Merz, B. and Blöschl, G., 2004. Flood risk assessment and associated
709 uncertainty. *Natural Hazards and Earth System Sciences*, 4(2): 295-308.
- 710 Arnaud, P. and Lavabre, J., 1999. Using a stochastic model for generating hourly hyetographs to
711 study extreme rainfalls. *Hydrological Sciences Journal*, 44(3): 433-446.
- 712 Arnell, N.W. and Reynard, N.S., 1996. The effects of climate change due to global warming on
713 river flows in Great Britain. *Journal of Hydrology*, 183(3-4): 397-424.
- 714 Arnell, N.W., Liu, C., Compagnucci, R., da Cunha, L., Hanaki, K., Howe, C., Mailu, G. &
715 Shiklomanov, I., 2001. *Climate Change 2001: Impacts, Adaptation and Vulnerability*.
716 IPCC.
- 717 Aronica, G., Bates, P.D. and Horritt, M.S., 2002. Assessing the uncertainty in distributed model
718 predictions using observed binary pattern information within GLUE. *Hydrological
719 Processes*, 16: 2001-2016.
- 720 Bates, P.D. and De Roo, A.P.J., 2000. A simple raster-based model for flood inundation
721 simulation. *Journal of Hydrology*, 236: 54-77.
- 722 Beven, 1987. Towards the use of catchment geomorphology in flood frequency predictions. *Earth
723 Surface Processes and Landforms*, 12: 69-82.
- 724 Beven, K. and Binley, A., 1992. The future of distributed models - model calibration and
725 uncertainty prediction. *Hydrological Processes*, 6(3): 279-298.
- 726 Blazkova, S. and Beven, K., 2002. Flood frequency estimation by continuous simulation for a
727 catchment treated as ungauged (with uncertainty). *Water Resources Research*, 38(8):
728 1139.
- 729 Blazkova, S. and Beven, K., 2004. Flood frequency estimation by continuous simulation of
730 subcatchment rainfalls and discharges with the aim of improving dam safety assessment
731 in a large basin in the Czech Republic. *Journal of Hydrology*, 292(1-4): 153-172.
- 732 Bullen Consultants, 2002. Standard of Protection Studies, River Cam and Granta (Draft Report),
733 UK Environment Agency.
- 734 Cadavid, L., Obeysekera, J.T.B. and Shen, H.W., 1991. Flood-frequency derivation from
735 kinematic wave. *Journal of Hydraulic Engineering*, 117(4): 489-510.
- 736 Cameron, D.S., Beven, K.J. and Tawn, J., 1999. Flood frequency estimation by continuous
737 simulation for a gauged upland catchment (with uncertainty). *Journal of Hydrology*,
738 219(3-4): 169-187.
- 739 Cameron, D.S., Beven, K. and Tawn, J., 2000. An evaluation of three stochastic rainfall models.
740 *Journal of Hydrology*, 228(1-2): 130-149.
- 741 Cernesson, F., Lavabre, J. and Masson, J.M., 1996. Stochastic model for generating hourly
742 hyetographs. *Atmospheric Research*, 42(1-4): 149-161.
- 743 Chetty, K. and Smithers, J., 2005. Continuous simulation modelling for design flood estimation in
744 South Africa: Preliminary investigations in the Thukela catchment. *Physics and Chemistry
745 of the Earth*, 30(11-16): 634-638.
- 746 Cunge, J.A., Holly Jr, F.A. and Verwey, A., 1976. *Practical aspects of computational river
747 hydraulics*. Pitman, London.
- 748 Dai, A., Fung, I.Y. and DelGenio, A.D., 1997. Surface observed global land precipitation
749 variations during 1900-88. *Journal of Climate*, 10(11): 2943-2962.

- 750 Dawson, R., Hall, J., Sayers, P., Bates, P., Rosu, C., 2005. Sampling-based flood risk analysis for
751 fluvial dike systems. *Stochastic Environmental Research and Risk Assessment*. 19(6):
752 388-402.
- 753 De Roo, A.P.J., Wesseling, C.G. and Van Deursen, W.P.A., 2000. Physically based river basin
754 modelling within a GIS: the LISFLOOD model. *Hydrological Processes*, 14(11-12): 1981-
755 1992.
- 756 De Roo, P.J., Gouweleeuw, B., Thielen, J., Bartholmes, J., Bongioannini-Cerlini, P., Todini, E.,
757 Bates, P.D., Horritt, M., Hunter, N., Beven, K.J., Pappenberger, F., Heise, E., Rivin, G.,
758 Hils, M., Hollingsworth, A., Holst, B., Kwadijk, J., Reggiani, P., Van Dijk, M., Sattler, K. &
759 Sprokkereef, E., 2003. Development of a European Flood Forecasting System.
760 *International Journal of River Basin Management.*, 1(1): 49-59.
- 761 DEFRA, 2002. *Flood Management - Capital Grant Allocations for Flood and Coastal Defence*.
762 <http://www.defra.gov.uk/environ/fcd/policy/grantaid.htm#scorecalc>
- 763 Diaz-Granados, M.A., Valdes, J.B. and Bras, R.L., 1984. A physically based flood frequency
764 distribution. *Water Resources Research*, 20(7): 995–1002.
- 765 Eagleson, P.S., 1972. Dynamics of Flood Frequency. *Water Resources Research*, 8(4): 878-898.
- 766 Easterling, D.R. et al., 2000. Observed variability and trends in extreme climate events: A brief
767 review. *Bulletin of the American Meteorological Society*, 81(3): 417-425.
- 768 Estrela, T. and Quintas, L., 1994. Use of a GIS in the modelling of flows on floodplains. In: W.R.
769 White and J. Watts (Editors), *Proceedings of the 2nd International Conference on River
770 Flood Dynamics*. Wiley, Chichester.
- 771 Faulkner, D. and Wass, R., 2005. Flood estimation by continuous simulation in the Don
772 catchment, South Yorkshire, UK. *Water and Environment Journal*, 19(2): 78-84.
- 773 Franchini, M., Hashemi, A.M. and O'Connell, P.E., 2000. Climatic and basin factors affecting the
774 flood frequency curve: PART II - A full sensitivity analysis based on the continuous
775 simulation approach combined with a factorial experimental design. *Hydrology and Earth
776 System Sciences*, 4(3): 483-498.
- 777 Goel, N.K., Kurothe, R.S., Mathur, B.S. and Vogel, R.M., 2000. A derived flood frequency
778 distribution for correlated rainfall intensity and duration. *Journal of Hydrology*, 228: 56-67.
- 779 Groisman, P.Y., Knight, R.W., Karl, T.R., Easterling, D.R., Sun, B.M., Lawrimore, J.H., 2004.
780 Contemporary changes of the hydrological cycle over the contiguous United States:
781 Trends derived from in situ observations. *Journal of Hydrometeorology*, 5(1): 64-85.
- 782 Halcrow, 2003. *Audit of the Cam and Granta Hydraulic Model*, Report, UK Environment Agency.
- 783 Halcrow, 2004. *Rivers Cam and Granta Model Improvements: Model Construction and SOP
784 Assessment. Final Report.*, UK Environment Agency.
- 785 Hall, J.W., Tarantola, S., Bates, P.D. and Horritt, M.S., 2005. Distributed sensitivity analysis of
786 flood inundation model calibration, *Journal of Hydraulic Engineering* 131 (2): 117–126.
- 787 Hashemi, A.M., Franchini, M. and O'Connell, P.E., 2000. Climatic and basin factors affecting the
788 flood frequency curve: PART I-A simple sensitivity analysis based on the continuous
789 simulation approach. *Hydrology and Earth System Sciences*, 4(3): 463-482.
- 790 Hebson, C. and Wood, E.F., 1982. A derived flood frequency distribution using Horton order
791 ratios. *Water Resources Research*, 18(5): 1509–1518.
- 792 Horritt, M.S. and Bates, P.D., 2001. Predicting floodplain inundation: raster-based modelling
793 versus the finite-element approach. *Hydrological Processes*, 15(5): 825-842.

- 794 Hsieh, L.S., Hsu, M.H. and Li, M.H., 2006. An assessment of structural measures for flood-prone
795 lowlands with high population density along the Keelung River in Taiwan. *Natural*
796 *Hazards*, 37(1-2): 133-152.
- 797 Hunter, N.M., Horritt, M.S., Bates, P.D. and Werner, M.G.F., 2004. Theoretical and practical limits
798 to the use of storage cell codes for flood inundation modelling. In: D. Reeve (Editor),
799 Flood risk assessment. Institute of Mathematics and its Applications, Southend-on-Sea.
- 800 Huntington, T.G., 2006. Evidence for intensification of the global water cycle: Review and
801 synthesis. *Journal of Hydrology*, 319(1-4): 83-95.
- 802 Jakeman, A.J., Littlewood, I.G. and Whitehead, P.G., 1990. Computation of the instantaneous
803 unit hydrograph and identifiable component flows with application to two small upland
804 catchments. *Journal of Hydrology*, 117: 275-300.
- 805 Kuchment, L.S. and Gelfan, A.N., 2002. Estimation of extreme flood characteristics using
806 physically based models of runoff generation and stochastic meteorological inputs. *Water*
807 *International*, 27(1): 77-86.
- 808 Kurothe, R.S., Goel, N.K. and Mathur, B.S., 1997. Derived Flood Frequency Distribution for
809 correlated rainfall intensity and duration. *Water Resources Research*, 33(9): 2103-2107.
- 810 Lamb, R., 1999. Calibration of a conceptual rainfall-runoff model for flood frequency estimation by
811 continuous simulation. *Water Resources Research*, 35(10): 3103-3114.
- 812 Maskey, S., Guinot, V. and Price, R.K., 2004. Treatment of precipitation uncertainty in rainfall-
813 runoff modelling: a fuzzy set approach. *Advances in Water Resources*, 27(9): 889-898.
- 814 McMillan, H.K., 2006. End-to-end flood risk assessment: A coupled model cascade with
815 uncertainty estimation. Thesis, University of Cambridge.
- 816 McMillan, H.K. and Brasington, J. 2007. Reduced Complexity Strategies for Modelling Urban
817 Floodplain Inundation. *Geomorphology: In Press*. doi:10.1016/j.geomorph.2006.10.031
- 818 Merz, B., Kreibich, H., Thielen, A. and Schmidtke, R., 2004. Estimation uncertainty of direct
819 monetary flood damage to buildings. *Natural Hazards and Earth System Sciences*, 4(1):
820 153-163.
- 821 Nash, J.E., 1959. Systematic determination of unit hydrograph parameters. *Journal of*
822 *Geophysical Research*, 64: 111-115.
- 823 Nash, J.E. and Sutcliffe, J.V., 1970. River flow forecasting through conceptual models. 1. A
824 discussion of principles. *Journal of Hydrology*, 10: 282-290.
- 825 Onof, C., Faulkner, D. and Wheater, H.S., 1996. Design rainfall modelling in the Thames
826 catchment. *Hydrological Sciences Journal-Journal Des Sciences Hydrologiques*, 41(5):
827 715-733.
- 828 Osborn, T.J. and Hulme, M., 2002. Evidence for trends in heavy rainfall events over the UK. *Phil.*
829 *Trans. R. Soc. Lond. A*, 360(1796): 1313-1325.
- 830 Pandit, A. and Gopalakrishnan, G., 1996. Estimation of annual storm runoff coefficients by
831 continuous simulation. *Journal of Irrigation and Drainage Engineering-Asce*, 122(4): 211-
832 220.
- 833 Pappenberger, F., Beven, K., Hunter, N., Bates, P., Gouweleeuw, B., Thielen, J. & de Roo, A.,
834 1999. *A European Flood Forecasting System: The Implementation of a Methodology for*
835 *Estimating the Predictive Uncertainty of Flood Forecasts*.
- 836 Pappenberger, F., Beven, K.J., Hunter, N.M., Bates, P.D., Gouweleeuw, B.T., Thielen, J. & de
837 Roo, A.P.J., 2005a. Cascading model uncertainty from medium range weather forecasts
838 (10 days) through a rainfall-runoff model to flood inundation predictions within the
839 European Flood Forecasting System (EFFS). *Hydrology and Earth System Sciences*,
840 9(4): 381-393.

- 841 Robson, A. and Reed, D., 1999. Flood Estimation Handbook Volume 3: Statistical procedures for
842 flood frequency estimation. Institute of Hydrology, Wallingford.
- 843 Romanowicz, R. and Beven, K., 2003. Estimation of flood inundation probabilities as conditioned
844 on event inundation maps, *Water Resources Research* 39 (3) (2003), pp. 1061–1073.
- 845 Romanowicz, R., Beven, K. and Tawn, J., 1996. Bayesian calibration of flood inundation models.
846 In: M.G. Anderson, D.E. Walling and P.D. Bates (Editors), *Floodplain Processes*. Wiley,
847 Chichester.
- 848 Sattler, K. and Feddersen, H., 2005. Limited-area short-range ensemble predictions targeted for
849 heavy rain in Europe. *Hydrology and Earth System Sciences*. 9(4): 300-312.
- 850 Sefton, C.E.M. and Howarth, S.M., 1998. Relationships between dynamic response
851 characteristics and physical descriptors of catchments in England and Wales. *Journal of*
852 *Hydrology*, 211: 1-16.
- 853 Silverman, B.W., 1982. Kernel Density Estimation using the Fast Fourier Transform. *Journal of*
854 *the Royal Statistical Society Series C*, 31(1): 93-99.
- 855 Silverman, B.W., 1986. *Density estimation for statistics and data analysis. Monographs on*
856 *statistics and applied probability*. Chapman and Hall, London.
- 857 Staeger, T., Grieser, J. and Schonwiese, C.D., 2003. Statistical separation of observed global
858 and European climate data into natural and anthropogenic signals. *Climate Research*,
859 24(1): 3-13.
- 860 US Army Corps of Engineers, 2005. *HEC History*.
861 <http://www.hec.usace.army.mil/whoweare/history.html>
- 862 Walshaw, D., 1994. Getting the most from your extreme wind data: A step-by-step guide. *Journal*
863 *of Research of the National Institute of Standards and Technology*., 99(4): 399-411.
- 864 Woolhiser, D.A. and Liggett, J.A., 1967. Unsteady, one-dimensional flow over a plane- The rising
865 hydrograph. *Water Resources Research*. 3: 753-771.
- 866 Wheeler, H.S., 2006. Flood Risk and Flood Management. *Phil. Trans. R. Soc. Lond. A*, In Press.
- 867 Young, P.C., 2003. Top-down and data-based mechanistic modelling of rainfall-flow dynamics at
868 the catchment scale. *Hydrological Processes*, 17: 2195-2217.
- 869 Young, P.C. and Beven, K., 1991. Computation of the instantaneous unit hydrograph and
870 identifiable component flows with application to two small upland catchments - comment.
871 *Journal of Hydrology*, 129(1-4): 389-396.
- 872 Young, P.C. and Beven, K., 1994. Data-based mechanistic modelling and the rainfall-flow
873 nonlinearity. *Environmetrics*, 5(3): 335-363.
- 874 Yu, D. and Lane, S.N., 2006. Urban fluvial flood modelling using a two-dimensional diffusion-
875 wave treatment, part 2: development of a sub-grid-scale treatment. *Hydrological*
876 *Processes*, 20(7): 1567-1583.

877

878

Figures

879

880 **Figure 1:** Modelled Discharge: Return Period Relation. (a) Full Range. (b) Detail. Dashed Lines
881 show A. Discharge associated with 2001 flood, with return period estimated from
882 median and quartiles and B. Discharge associated with 100-year flood.

883

884 **Figure 2:** Design Hydrographs for the 1000-year return period, at the 5%, 50% and 95% points
885 of the cumulative distribution

886

887 **Figure 3:** Areas of Predicted Inundation at the 5%, 50% and 95% points of the cumulative
888 distribution of peak discharge magnitudes

889

890 **Figure 4:** Number of houses flooded (to any depth) as a function of return period and point of
891 peak discharge distribution

892

893 **Figure 5:** Modelled Discharge: Return Period Relation, using single rainfall series. (a) Full
894 Range. (b) Detail. Dashed Line shows discharge associated with 2001 flood, with
895 return period estimated from median and quartiles.

896

897 **Figure 6:** Modelled Discharge: Return Period Relation, using optimised rainfall-runoff model
898 parameters. (a) Full Range. (b) Detail. Dashed Line shows discharge associated with
899 2001 flood, with return period estimated from median and quartiles.

900

901 **Figure 7:** Areas of Predicted Inundation at the 5%, 50% and 95% points of the cumulative
902 distribution of peak discharge magnitudes for the 100-year flood, using three
903 alternative methods to calculate uncertainty bounds.

904

905 **Figure 8:** Variation in inundation envelope: Comparison of (a) Uncertainty in rainfall and rainfall-
906 runoff model parameters and (b) Uncertainty associated with floodplain model channel
907 friction parameter

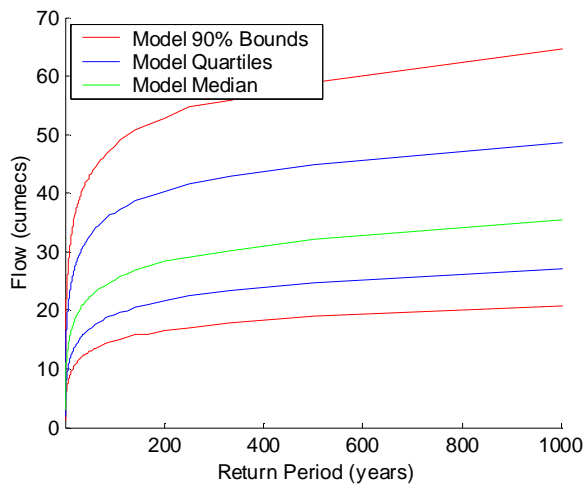
908

909 **Figure 9:** Comparison in 100-year flood envelopes predicted using the proposed End-to-End
910 method versus a standard statistical method using the 1D ISIS flood model

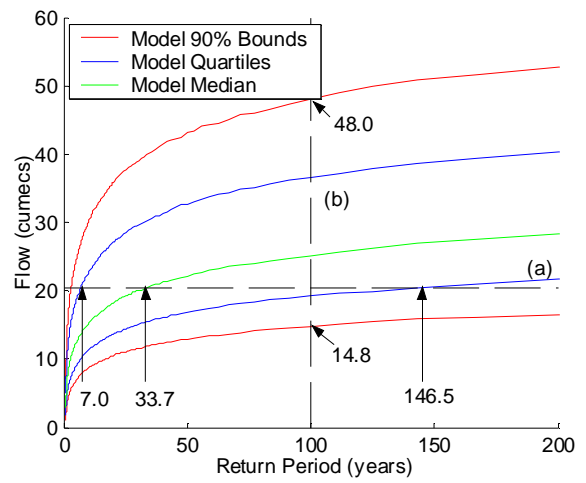
911

912

A



B



913

914

915

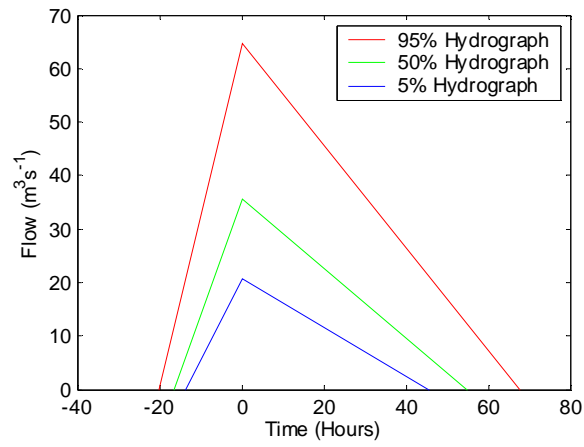
916

917

918

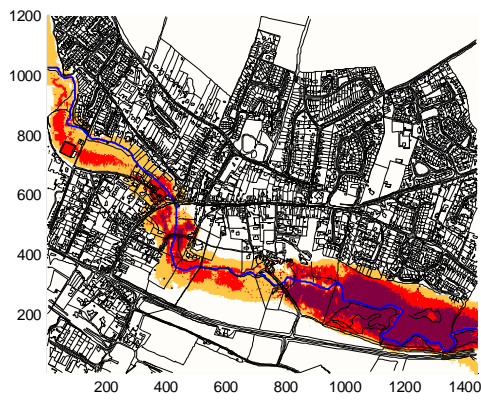
Figure 1: Modelled Discharge: Return Period Relation. A. Full Range. B. Detail. Dashed Lines show (a) Discharge associated with 2001 flood, with return period estimated from median and quartiles and (b) Discharge associated with 100-year flood.

919

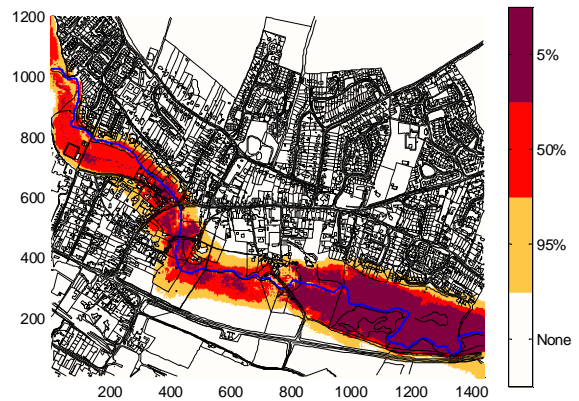


920
921
922
923

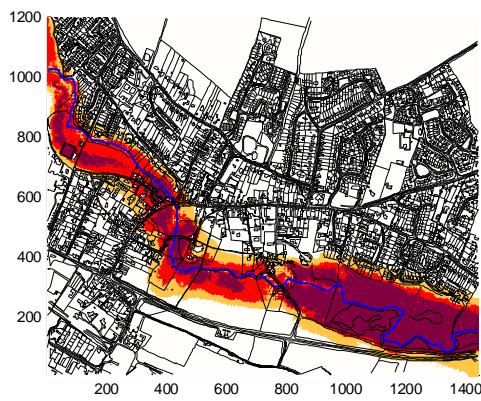
Figure 2: Design Hydrographs for the 1000-year return period, at the 5%, 50% and 95% points of the cumulative distribution



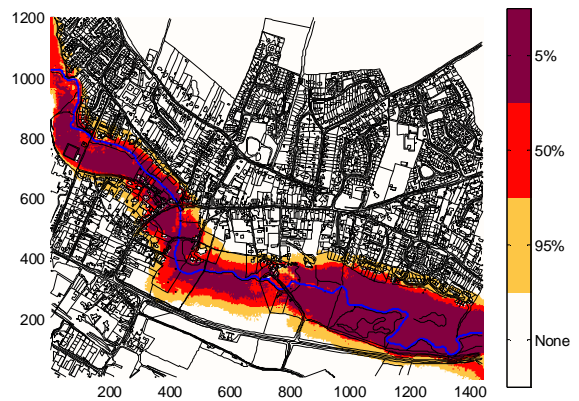
(a) 10-Year Return Period



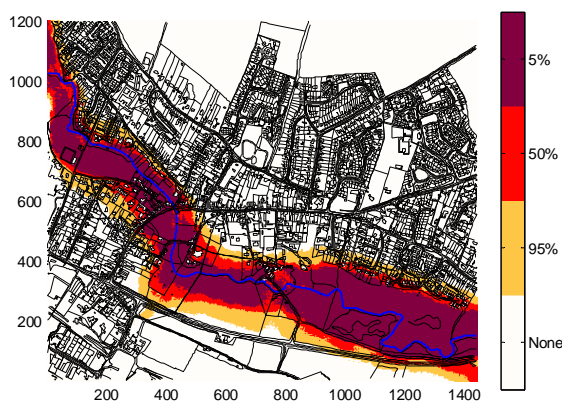
b) 50-Year Return Period



c) 100-Year Return Period



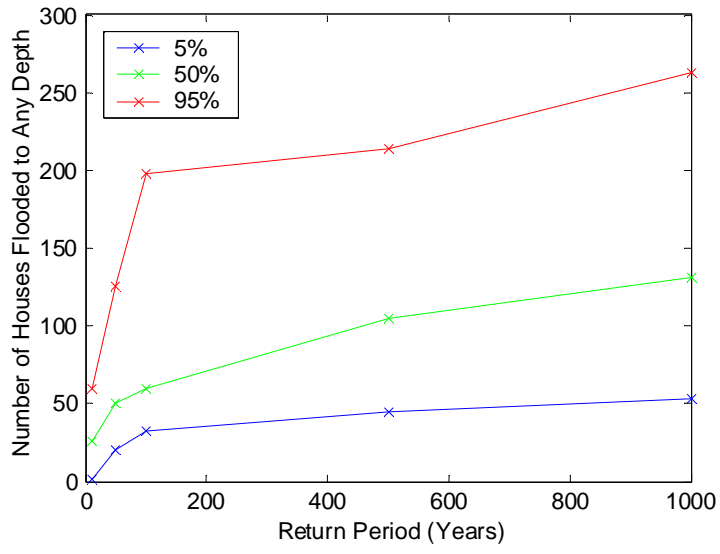
d) 500-Year Return Period



e) 1000-Year Return Period

925
926
927
928

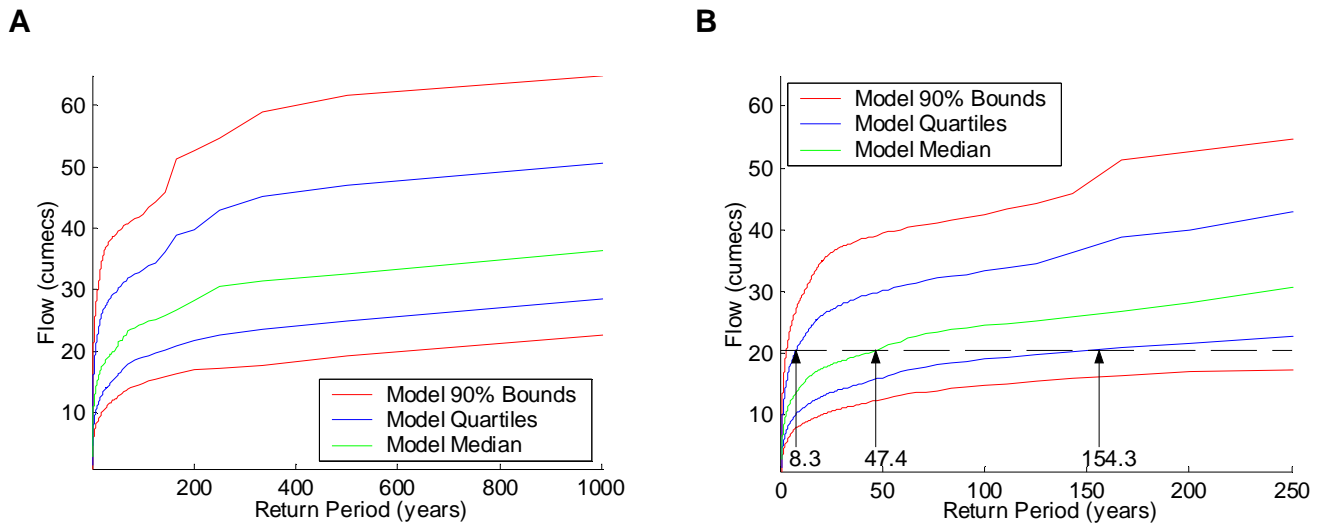
Figure 3: Areas of Predicted Inundation at the 5%, 50% and 95% points of the cumulative distribution of peak discharge magnitudes



929
 930
 931
 932
 933
 934

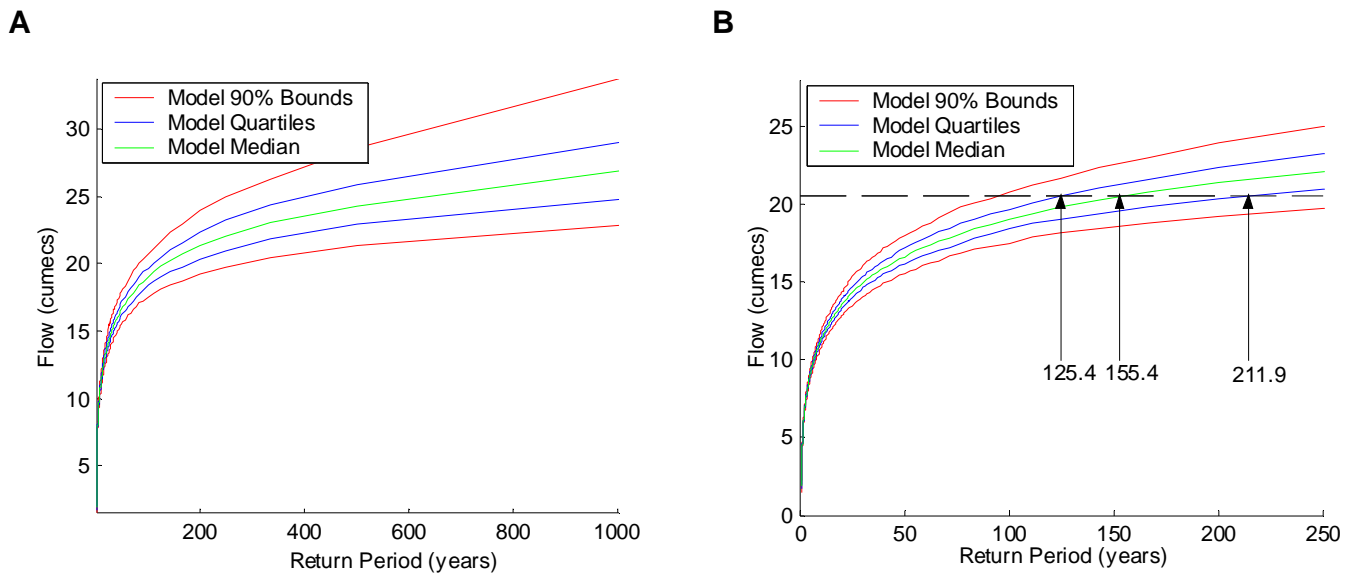
Figure 4: Number of houses flooded (to any depth) as a function of return period and percentage point of peak discharge distribution

935



936
937
938
939

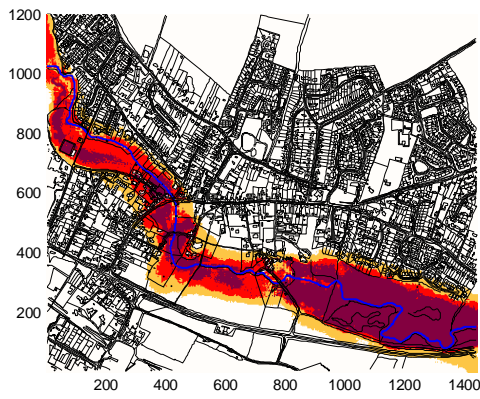
Figure 5: Modelled Discharge: Return Period Relation, using single rainfall series A. Full Range. B. Detail. Dashed Line shows discharge associated with 2001 flood, with return period estimated from median and quartiles.



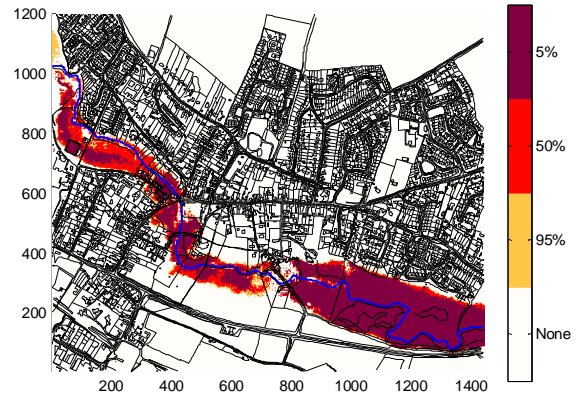
941
942
943
944
945

Figure 6: Modelled Discharge: Return Period Relation, using optimised rainfall-runoff model parameters. A. Full Range. B. Detail. Dashed Line shows discharge associated with 2001 flood, with return period estimated from median and quartiles.

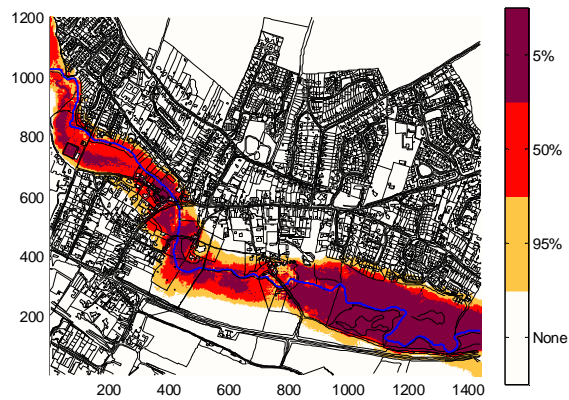
946



a) Original Analysis Repeated for Comparison



b) Single Set of Rainfall-Runoff Model Parameters



c) Single Rainfall Series

947

948

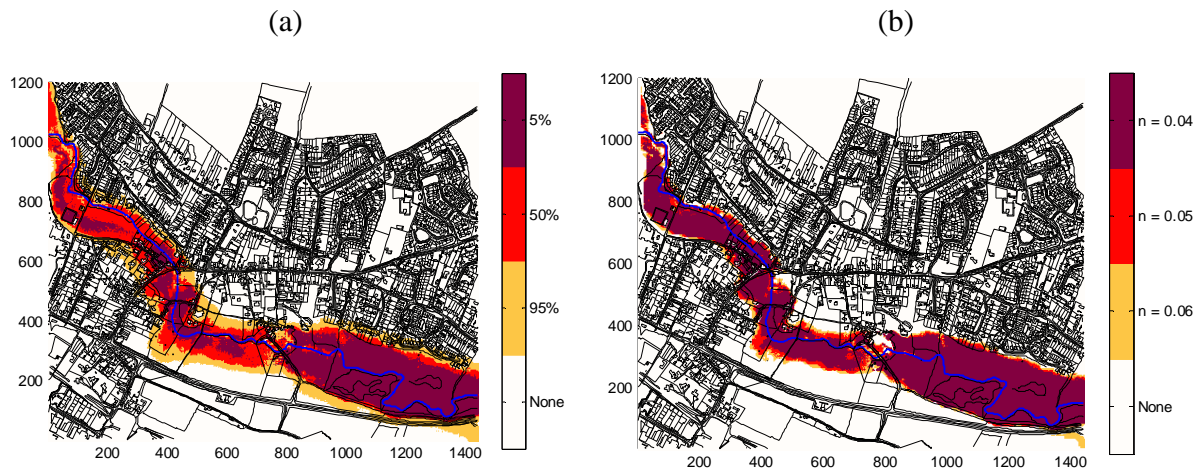
949

950

951

Figure 7: Areas of Predicted Inundation at the 5%, 50% and 95% points of the cumulative distribution of peak discharge magnitudes for the 100-year flood, using three alternative methods to calculate uncertainty bounds.

952



953

954

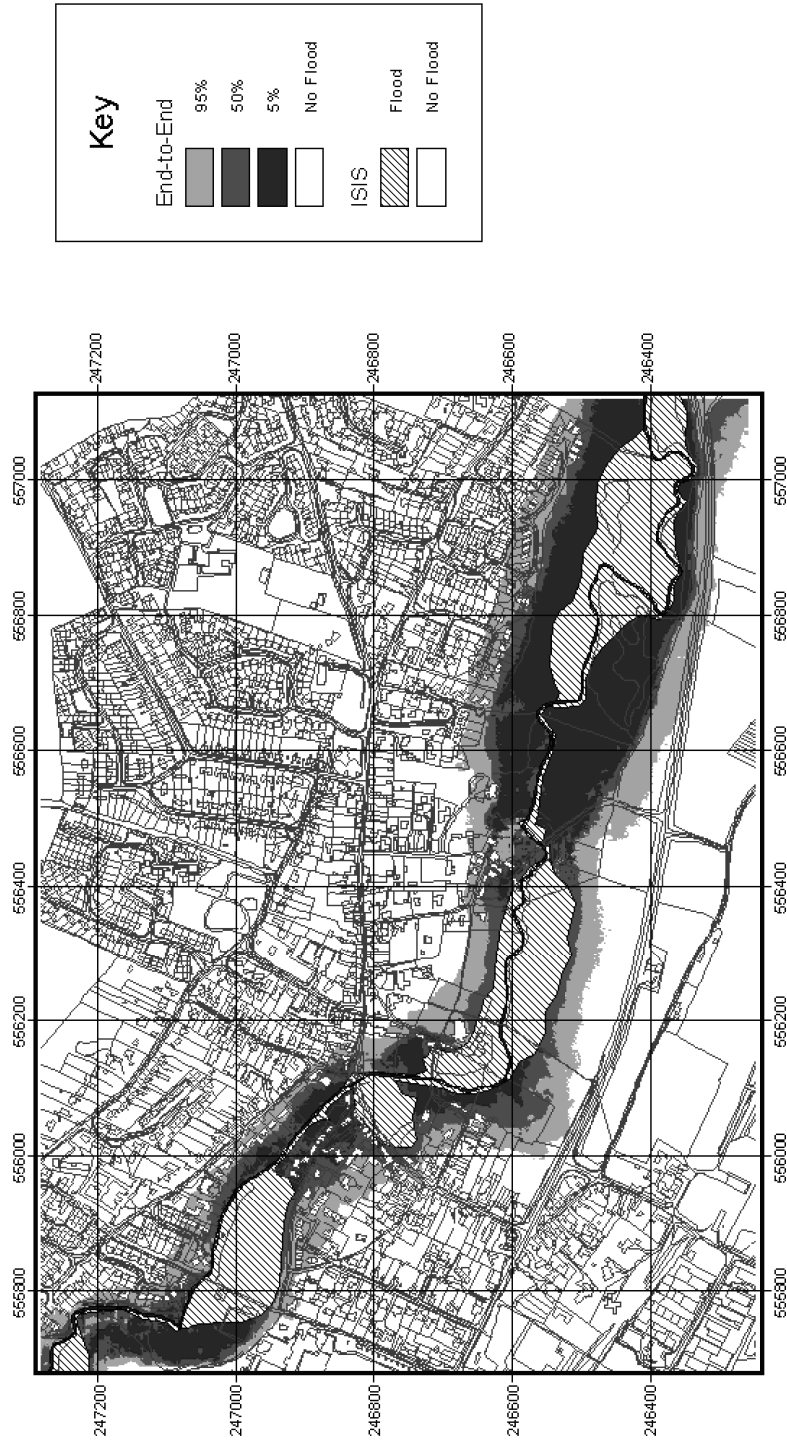
955

956

Figure 8: Variation in inundation envelope: Comparison of (a) Uncertainty in rainfall and rainfall-runoff model parameters and (b) Uncertainty associated with floodplain model channel friction parameter

957

958



959
 960
 961
 962
 963
 964

Figure 9: Comparison in 100-year flood envelopes predicted using the proposed End-to-End method versus a standard statistical method using the 1D ISIS flood model